Journal of Hydrology 536 (2016) 496–513

Contents lists available at ScienceDirect

Journal of Hydrology

journal homepage: www.elsevier.com/locate/jhydrol

Rainfall/runoff simulation with 2D full shallow water equations: Sensitivity analysis and calibration of infiltration parameters

Javier Fernández-Pato [a,*], Daniel Caviedes-Voullième [a,b], Pilar García-Navarro [a]

[a] LIFTEC-CSIC, University of Zaragoza, Spain
[b] Chair for Hydrology and Water Resource Managment, Brandenburg University of Technology Cottbus-Senftenberg, Germany

ARTICLE INFO

Article history:
Received 21 December 2015
Received in revised form 2 March 2016
Accepted 11 March 2016
Available online 18 March 2016
This manuscript was handled by Konstantine P. Georgakakos, Editor-in-Chief, with the assistance of Marco Borga, Associate Editor

Keywords:
Finite volumes
Shallow-water equations
Hydrologic modeling
Infiltration models
Rain-runoff generation

SUMMARY

One of the most difficult issues in the development of hydrologic models is to find a rigorous source of data and specific parameters to a given problem, on a given location that enable reliable calibration. In this paper, a distributed and physically based model (2D Shallow Water Equations) is used for surface flow and runoff calculations in combination with two infiltration laws (Horton and Green–Ampt) for estimating infiltration in a watershed. This technique offers the capability of assigning a local and time-dependent infiltration rate to each computational cell depending on the available surface water, soil type or vegetation. We investigate how the calibration of parameters is affected by transient distributed Shallow Water model and the complexity of the problem. In the first part of this work, we calibrate the infiltration parameters for both Horton and Green–Ampt models under flat ponded soil conditions. Then, by means of synthetic test cases, we perform a space-distributed sensitivity analysis in order to show that this calibration can be significantly affected by the introduction of topography or rainfall. In the second part, parameter calibration for a real catchment is addressed by comparing the numerical simulations with two different sets of experimental data, corresponding to very different events in terms of the rainfall volume. We show that the initial conditions of the catchment and the rainfall pattern have a special relevance in the quality of the adjustment. Hence, it is shown that the topography of the catchment and the storm characteristics affect the calibration of infiltration parameters.

1. Introduction

The field of hydrology is of great importance in all environmental-related sciences, as Civil Engineering or Geology because of the fundamental relevance of water availability, flood risks, urban sewer systems or water quality control. In particular, hydrologic water losses play a relevant role in the spatial distribution and temporal evolution of the runoff water in real catchments. Typically, the most important component of the hydrologic water loss is the infiltration process.

In hydrologic modeling lumped models provide no information about the spatial variations occurring within a system. They consider all the hydrologic variables uniform in space (at least in large regions) and give an outlet response to inlet data (usually rain). On the other hand, fully dynamic distributed models provide a full description of the phenomena, that is, a detailed description of the catchment topography, computation of surface water depth and flow discharge and variation in space of infiltration and precipitation. They consider that runoff generation is a hydrologic response, continuous in space and time, to a hydraulic phenomenon. If properly calibrated, the model should have better predictive capabilities with less parameters.

The modeling of infiltration can be performed in different forms. When focusing on subsurface processes, Richards equation can be used and the infiltration is derived from the surface–subsurface water exchange (Richards, 1931). On the other hand, if the focus is on overland flow, infiltration participates as a water volume loss that can be formulated using empirical laws. The present work belongs to this category. The most used infiltration methods in Hydrology are the SCS-CN (USDA, 1986), Philip (Philip, 1969), Horton (Horton, 1933, 1939) and Green–Ampt (Green and Ampt, 1911) models. Among these, the present work is concerned with the analysis of the potential superiority of Horton and Green–Ampt methods in the simulation of rainfall/runoff events in a real basin where the SCS method was used and found to be inadequate (Caviedes-Voullième et al., 2012). Both require as input data a set of parameters dependent mainly (theoretically) on the soil properties. A proper calibration of these parameters is essential to achieve

* Corresponding author at: Ed. Torres Quevedo, María de Luna 3, CP 50018 Zaragoza, Spain. Tel.: +34 876555057; fax: +34 976761882.
E-mail address: jfpato@unizar.es (J. Fernández-Pato).

http://dx.doi.org/10.1016/j.jhydrol.2016.03.021
0022-1694/

an accurate result for the infiltration rate and the surface runoff (Van den Putte et al., 2013). The main advantage of the Green–Ampt model is the physical basis of its parameters. The original model was updated by Mein and Larson (1973) in order to consider the ponding time of the soil under a steady rainfall. Unsteady rainfall was first covered by Chu (1978) in order to predict surface runoff under natural storm patterns. Green–Ampt model has been successfully applied to model rainfall–runoff processes in natural catchments (Esteves et al., 2000; Simons et al., 2014). A recent and conscientious comparison among models using Green–Ampt method is reported in Kale and Sahoo (2011). On the other hand, the Horton model makes use of empirically derived parameters to characterize the soil infiltration process, so they are not directly related with the soil characteristics. An overview of the recent watershed-scale models for infiltration and runoff calculation can be found in Migliaccio and Srivastav (2007). They lead to the idea that hydrologic modeling is constantly taking advantage of new tools (GIS, remote sensing) and the advances in computation capacity, which lead to the incorporation of more precise calibration–validation processes. Singh and Woolhiser (2002) provided a very detailed historical perspective of the different techniques of modeling and measuring watersheds, stating that the global trend is to develop hydrologic models embedded in other larger models, involving several knowledge areas.

Overland flow is solved in the present work by means of the 2D SWE. The numerical solution is calculated through an explicit, first-order upwind finite volume scheme (Murillo and García-Navarro, 2010; Murillo et al., 2007). The main objective is to demonstrate the ability of that system of equations to reproduce rainfall/runoff events instead of the more widely used simplified formulations of the overland flow such as kinematic-wave or diffusion-wave (Cea et al., 2010; Kim and Seo, 2013; López-Barrera et al., 2011), or even simpler lumped runoff models. Flows in this study are mostly driven by strong topographic gradients, which require a rather high grid resolution to be represented at the discrete level. However, because the cost per cell may be significantly higher in a high order scheme, in the presence of a rather fine spatial discretization, it results more efficient to use a first order scheme, as is the case here. First order schemes are already TVD (hence free from spurious oscillations) provided that they are well designed to ensure a discrete balance between fluxes and source terms. Finally, the continuous and ubiquitous presence of wet/dry fronts in real rain events makes higher order schemes not ideal, since wet/dry fronts require, at the most second-order accuracy. These are the reasons for choosing a first-order scheme for the application presented.

It should be noted that few works include 2D SWE-based models combined with empirical infiltration laws distributed in space to study the surface runoff in real catchments. 2D SWE represent a complete mathematical description of the physical phenomena related to surface water at catchment level. By taking advantage of the flow information provided by this strategy, the infiltration is locally calculated in each cell, leading to a cell-based computation of this magnitude and thence to a fine calibration of the infiltration parameters. Therefore, one of the motivations for this work is to show that the calibration of the infiltration parameters for both Horton and Green–Ampt models can depend on the topography of the problem as well as on the storm pattern characteristics.

The methodology for this work is divided into two main parts. In the first part, given a set of Green–Ampt parameters corresponding to a soil type, the best choice of Horton parameters is found so that the same cumulative infiltration is achieved by both models in the same time. These sets are then used in next simulations. Then, a sensitivity analysis is performed through several test cases in order to check the influence of the topography features (slope, roughness, water storage areas) and rainfall characteristics on the relative response of the models using always the same set of infiltration parameters. In the second part of this work, a real catchment simulation is carried out for three storm events, very different in terms of duration and water volume. The fitting to experimental data provides an estimation of the infiltration parameters for both Horton and Green–Ampt models.

The structure of the paper is as follows: after a brief overview of surface flow and empirical infiltration models (Horton and Green–Ampt) (Section 2), a set of test cases for calibration and sensitivity analysis is presented in Section 3. A validation of the full shallow water model with infiltration is done by means of the calibration of a real catchment with experimental data (Section 4). A study of different infiltration areas depending of the soil types and vegetation cover is also presented in this section.

2. Mathematical model

2.1. Surface water model

In this paper, surface flow is simulated by means of the 2D shallow-water equations (Murillo et al., 2007), which can be expressed as in Eq. (1):

$$\frac{\partial \mathbf{U}}{\partial t}+\frac{\partial \mathbf{F}(\mathbf{U})}{\partial x}+\frac{\partial \mathbf{G}(\mathbf{U})}{\partial y}=\mathbf{S}+\mathbf{H}+\mathbf{M} \tag{1}$$

where

$$\mathbf{U}=(h,q_x,q_y)^T \tag{2}$$

are the conserved variables, being h the water depth (m) and $q_x=hu$ and $q_y=hv$ the unit discharges (m^2/s), with u and v (m/s) the depth averaged components of the velocity vector $\mathbf{u}$ along the x and y coordinates respectively. The fluxes of these conserved variables are given by

$$\mathbf{F}=\left(q_x,\frac{q_x^2}{h}+\frac{1}{2}gh^2,\frac{q_xq_y}{h}\right)^T,\quad \mathbf{G}=\left(q_y,\frac{q_xq_y}{h},\frac{q_y^2}{h}+\frac{1}{2}gh^2\right)^T \tag{3}$$

where g (m/s^2) represents the acceleration due to gravity. The source terms of the system are split into three kind of terms. The term $\mathbf{S}$ corresponds to friction and it is defined as

$$\mathbf{S}=(0,\ -ghS_{fx},\ -ghS_{fy})^T \tag{4}$$

where S_{fx},S_{fy} are the friction slopes in the x and y direction respectively, usually written in terms of the Manning's roughness coefficient n (s m$^{-1/3}$):

$$S_{fx}=n^2u\sqrt{u^2+v^2}/h^{4/3},\quad S_{fy}=n^2v\sqrt{u^2+v^2}/h^{4/3} \tag{5}$$

The term $\mathbf{H}$ is defined as

$$\mathbf{H}=\left(0,\ -gh\frac{\partial z}{\partial x},\ -gh\frac{\partial z}{\partial y}\right)^T \tag{6}$$

and accounts for the variation of the pressure force along the bottom in both x and y directions, formulated in terms of the bed slopes of the bottom level z (m).

Finally, the term $\mathbf{M}$ represents the mass sources and sinks due to rainfall and infiltration processes:

$$\mathbf{M}=(R-f,0,0)^T \tag{7}$$

being R (m/s) the rainfall intensity and f (m/s) the infiltration rate.

System (1) is time dependent, non linear, and contains source terms. Under the hypothesis of dominant advection it can be classified and numerically dealt with as belonging to the family of hyperbolic systems. The mathematical properties of (1) include the existence of a Jacobian matrix, $\mathbf{J_n}$, of the flux normal to an

Table 1
Infiltration parameters sets.

Infiltration model	Parameter 1	Parameter 2	Parameter 3
Horton	$k = 2.43 \cdot 10^{-3}$ s^{-1}	$f_c = 3.272 \cdot 10^{-5}$ m/s	$f_0 = 1.977 \cdot 10^{-4}$ m/s
Green–Ampt	$K = 3.272 \cdot 10^{-5}$ m/s	$\Psi = 0.0495$ m	$\Delta\theta = 0.38$ m^3/m^3

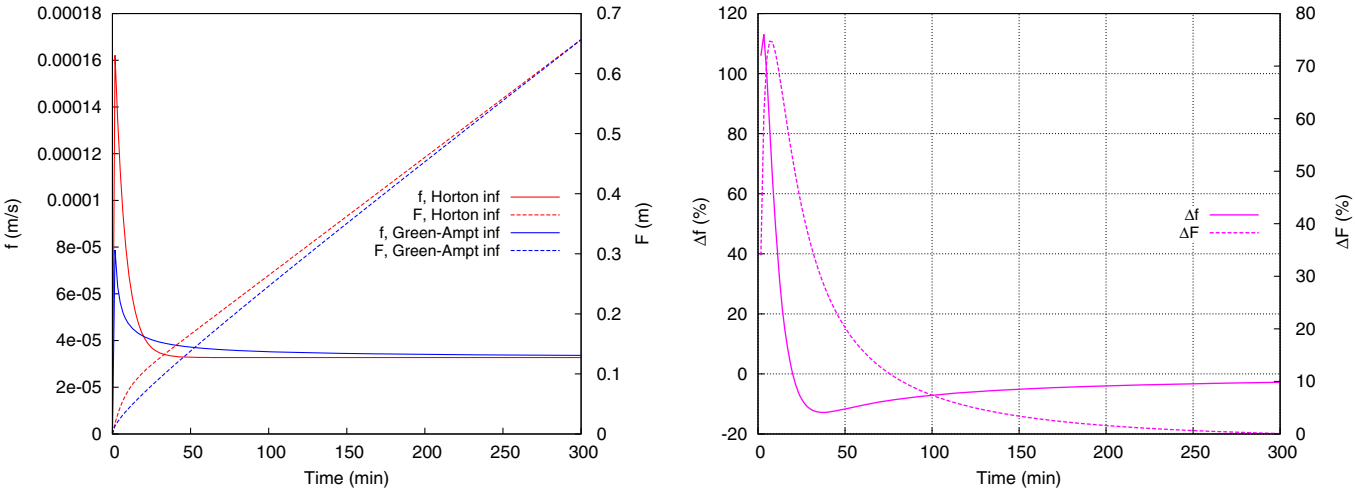

Fig. 1. Infiltration rate and cumulative infiltration curves (left) and relative differences between models in f and F (right) for Case 0.

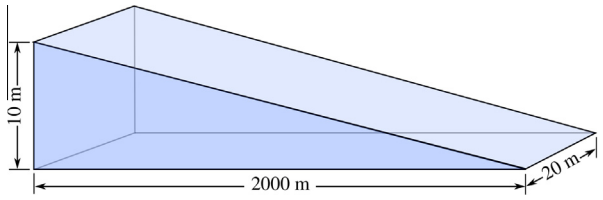

Fig. 2. Case 1 topography.

Table 2
Cases 1-1 to 1-5 rainfall characteristics and rain volume.

Case	Rainfall pattern	Rain volume (m^3)
1-1	Uniform	75,000
1-2	Non-uniform	75,000
1-3	Non-uniform	56,250
1-4	Uniform	35,000
1-5	Non-uniform	43,000

outward direction given by the unit vector $\mathbf{n}, \mathbf{E}\cdot\mathbf{n} = \mathbf{F}n_x + \mathbf{G}n_y$ (Murillo and García-Navarro, 2010) defined as

$$\mathbf{J_n} = \frac{\partial \mathbf{E}\cdot\mathbf{n}}{\partial \mathbf{U}} = \frac{\partial \mathbf{F}}{\partial \mathbf{U}}n_x + \frac{\partial \mathbf{G}}{\partial \mathbf{U}}n_y \tag{8}$$

The presented equations are solved by an explicit, upwind, first-order accurate finite volume scheme described in Murillo and García-Navarro (2010). The numerical model is designed to solve the flow variables only in the surface cells covered by water (wet cells). The wet/dry fronts are well tracked leading to stable solutions with machine accuracy mass error.

2.2. Infiltration laws

Infiltration is the process by which surface water enters the soil. This process is mainly governed by two forces: gravity and capillarity action. In this section, two widely used laws are presented, Horton and Green–Ampt infiltration methods. Both formulate the infiltration rate and cumulative infiltration volume in terms of several soil parameters.

2.2.1. Horton model

Horton's infiltration model (Horton, 1933) suggests an exponential equation for modeling the soil infiltration capacity or maximum infiltration rate f_p (m/s):

$$f_p(t) = f_c + (f_0 - f_c)e^{-kt} \tag{9}$$

where f_0 and f_c are the initial and final infiltration capacities (m/s) and k represents the rate of decrease in the capacity (s^{-1}).

The parameters f_0 and k have no clear physical basis, so they must be estimated from calibrating the model against experimental data. A good source for experimental values of these parameters for different types of soils can be found in Rawls et al. (1976) and is summarized in ASCE (1996).

Eq. (9) assumes an unlimited water supply at the surface. This means that it has to be applied after surface ponding. It is important to highlight the difference between the infiltration capacity f_p and the infiltration rate f. In absence of ponding surface water, a rain event starting with a weak rainfall intensity ($R \leqslant f_p$), then all the rain will completely infiltrate into the soil. On the other hand, if the rain intensity exceeds the soil infiltration capacity the surface becomes ponded and Horton law (9) applies. Therefore:

$$f(t) = \begin{cases} R(t) & \text{if } R(t) \leqslant f_p(t) \\ f_p(t) & \text{if } R(t) > f_p(t) \end{cases} \tag{10}$$

The cumulative infiltration $F(t)$, up to time t, can be calculated by integrating the infiltration capacity f as:

$$F(t) = \int_0^t f(t)dt = f_c t + \frac{f_0 - f_c}{k}\left(1 - e^{-kt}\right) \tag{11}$$

2.2.2. Green–Ampt model

The Green–Ampt model (Green and Ampt, 1911; Mein and Larson, 1973) is based on parameters which have physical meaning and can be estimated from soil properties. A good source of the most common soil parameters is found in Rawls and Brakensiek (1983).

The Green–Ampt model approximates the soil infiltration capacity as follows:

$$f_p(t) = K_s + \frac{K_s \Psi \Delta\theta}{F(t)} \tag{12}$$

being K_s (m/s) the saturated hydraulic conductivity, Ψ (m) the average suction head at the wetting front and $\Delta\theta = \theta_s - \theta_i$ (m^3/m^3) the difference between the soil porosity θ_s (m^3/m^3) and the initial volumetric water content θ_i (m^3/m^3).

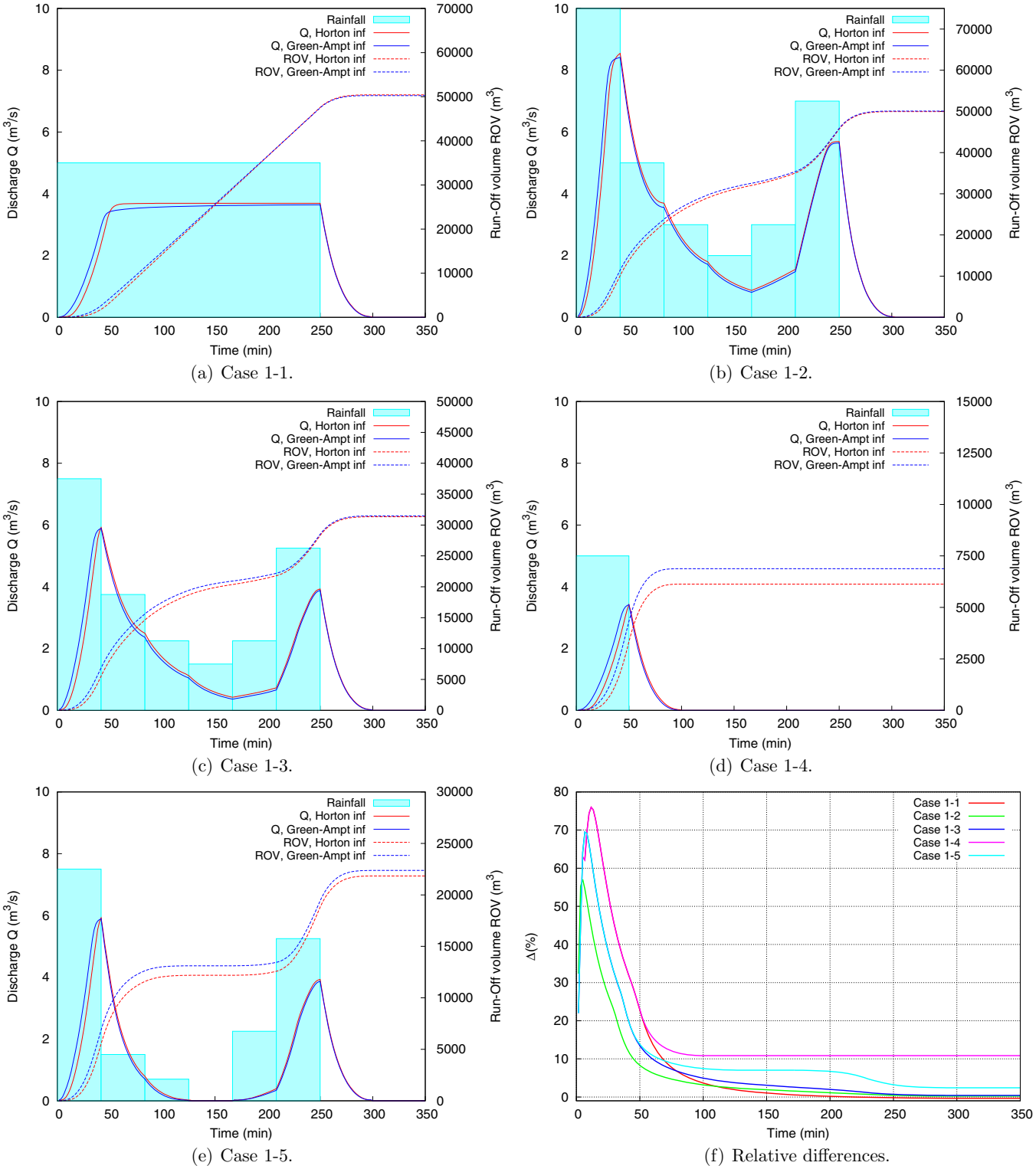

(a) Case 1-1. (b) Case 1-2. (c) Case 1-3. (d) Case 1-4. (e) Case 1-5. (f) Relative differences.

Fig. 3. Cases 1-1 to 1-5. Outlet hydrographs for sensitivity to rainfall analysis.

Using (12) and the relationship between the infiltration capacity and the cumulative infiltration $f_p = \frac{dF}{dt}$, it is possible to reach an equation for F:

$$K_s t = F(t) - \Psi\Delta\theta \ln\left[1 + \frac{F(t)}{\Psi\Delta\theta}\right] \tag{13}$$

Solving F in (13) requires an iterative procedure (e.g. Newton–Raphson method).

Eqs. (12) and (13) assume that the soil is ponded from the beginning. Eq. (10) is also applicable for the Green–Ampt model. Additional considerations are taken into account in order to model an unsteady storm pattern where ponding may occur following Te Chow et al. (1988).

3. Synthetic test cases

A set of synthetic test cases is presented now for a better understanding of the infiltration response to rainfall, infiltration parameters and topography variations. Several variations are performed on each case to study the sensitivity to the aforementioned issues.

3.1. Case 0: infiltration parameters calibration

First of all, the soil type is the only factor considered. A basic fitting for infiltration parameters is presented. The case consists of infiltration over a horizontal ponded soil. The goal is to get an approximated equivalence between two sets of parameters of Horton (k, f_c, f_0) and Green–Ampt $(K, \Psi, \Delta\theta)$ infiltration models in ideal conditions.

The fitting procedure is summarized as follows:

1. The starting point consists of choosing the Green–Ampt parameters $K, \Delta\theta$ and Ψ so that they are adequate to represent the assumed soil characteristics and initial water content.
2. It is assumed that both the Horton's model final infiltration capacity f_c and the soil hydraulic conductivity K_s reach the same value representing the behavior at large times $(t \to T)$.
3. The initial Horton's infiltration rate f_0 is set to the numerical Green–Ampt initial rate $f(t = 0)$.
4. The exponential decay constant k in Horton model is fitted in order to achieve the same final cumulative infiltration volume in both models at a time T.

Following these steps, a set of parameters (Table 1) for each infiltration model has been obtained corresponding to a sandy soil type. In order to illustrate the calibration results, Fig. 1 shows the

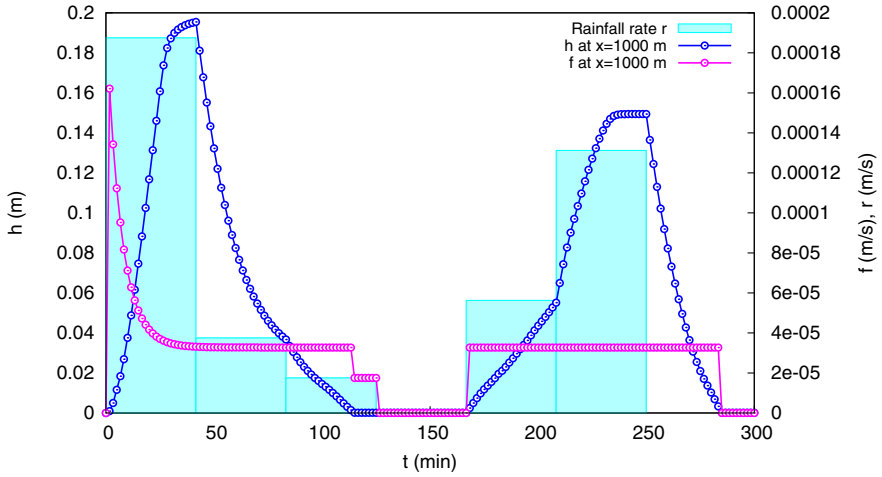

(a) f and h curves for Horton model.

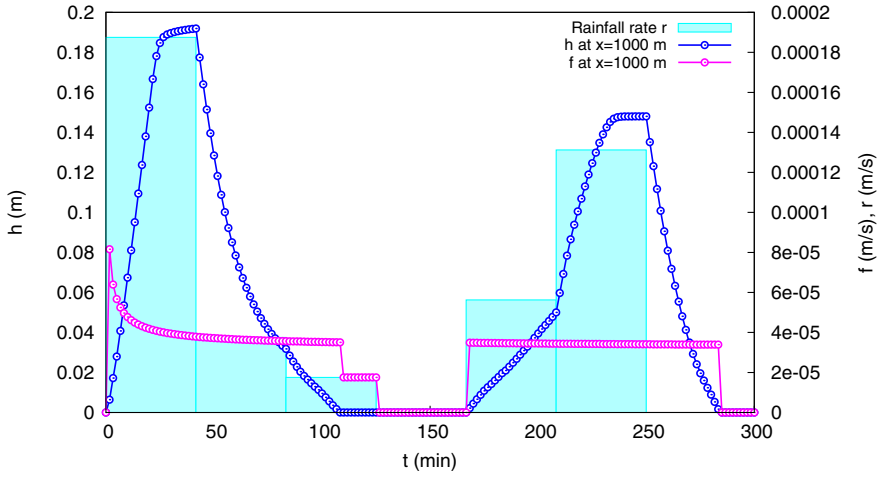

(b) f and h curves for Green-Ampt model.

Fig. 4. Case 1-5. Water depth and infiltration rate curves for Horton and Green–Ampt models.

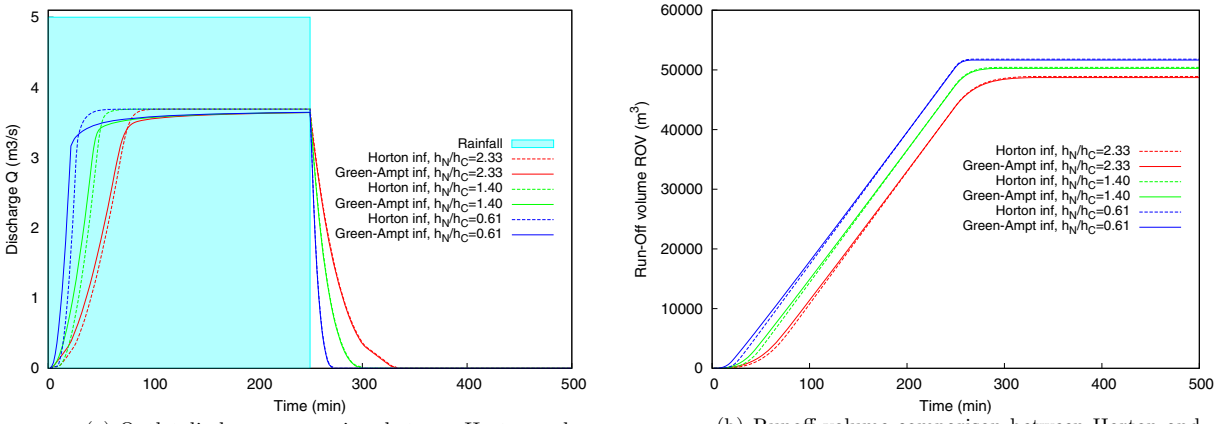

(a) Outlet discharge comparison between Horton and Green-Ampt infiltration models.

(b) Runoff volume comparison between Horton and Green-Ampt infiltration models.

Fig. 5. Case 1. Flow profile variations.

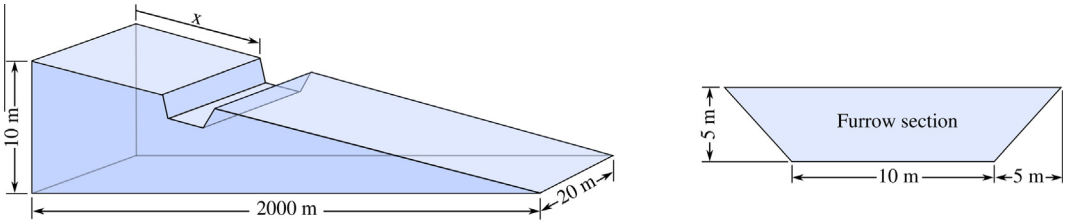

Fig. 6. Case 2 topography.

Table 3
Case 2 setups.

Case	Storage area position
2-100	$x = 100$ m
2-1900	$x = 1900$ m

infiltration rate and cumulative infiltration curves for the infiltration parameters considered.

The relative differences in f and F between infiltration models are also presented in Fig. 1 in terms of the magnitudes $\Delta f(\%)$ and $\Delta F(\%)$, defined as follows:

$$\Delta f(\%) = 100\frac{f_H - f_{GA}}{f_{GA}}, \quad \Delta F(\%) = 100\frac{F_H - F_{GA}}{F_{GA}} \tag{14}$$

3.2. Case 1: uniform inclined plane

A uniform slope plane of 0.005 is considered in this case (see Fig. 2). The Manning's roughness coefficient is set to 0.03 $s/m^{1/3}$. The initial conditions for the surface water equations are zero water depth and zero discharge everywhere, that is, dry surface conditions. Water enters the domain only through rainfall, which is assumed to be constant in space, hence there are not inlet boundaries. The only open boundary is at the outlet (downslope) and free outflow is assumed. Two studies are performed with this case: an analysis of the sensitivity to water availability and a study of the effects of slope and roughness variations.

3.2.1. Sensitivity to water availability

The motivation for the tests is to check if the response of the two models is the same using the chosen parameters. For this purpose, different rain conditions are considered (see Table 2). In Cases 1-1 to 1-3 the rainfall conditions guarantee full water availability at downslope during the period (0–300 min), which matches with the period used for calibration in Case 0. This enforces the same conditions of water availability for infiltration as in the calibration process. The results are presented in Fig. 3. The results for Cases 1-1 to 1-3 show that, while the outlet hydrographs for Horton and Green–Ampt models are slightly different, the same runoff volume (ROV) is achieved. Hence, the calibration of the infiltration parameters performed in a flat ponded soil remains applicable in a mild slope if water is available for infiltration. In addition, neither the storm pattern (Case 1-2, Fig. 3(b)) nor the rainfall volume (Case 1-3, Fig. 3(c)) affect the calibration of the infiltration parameters.

On the other hand, it is possible that the rainfall pattern is not adequate for the continuous runoff generation until a time near to the calibration point ($t = 300$ min). This situation can be reached in two ways. The first one consists of a short rainfall duration (Case 1-4, Fig. 3(d)). In this case, the runoff finishes long before the calibration point. The second possibility corresponds to Case 1-5 and it is shown in Fig. 3(e). In this case, the storm pattern presents a temporal distribution which generates a discontinuity in the runoff due to a reduction of the water availability for infiltration in the 0–300 min period. As shown in Fig. 3(d) and (e), both cases present differences in the outlet runoff volumes. The reason for this behavior is that the period of time with available water is less than the one for what the calibration has been performed (Case 0). Hence, the calibration of the infiltration parameters is not valid in this kind of situations.

Fig. 3(f) shows the evolution in time of the relative difference between the runoff volume for both infiltration models, defined as follows:

$$\Delta(\%) = 100\frac{ROV_{GA} - ROV_H}{ROV_{GA}} \tag{15}$$

In the light of these results, it is clear that the greater the difference between water availability time and calibration time, the greater the difference between infiltration models (Cases 1-4 and 1-5). From Fig. 3(f), it is clearly seen that there are huge differences in outlet hydrographs produced by both models at early times of the simulation. This is due to the fact that the infiltration rates of both models differ at this time, since the fitting time for the models has not been yet reached. When approaching this calibration point ($t = 300$ min) the magnitude Δ decreases in general and tends to zero in cases with full water availability during this time (Cases 1-1, 1-2 and 1-3). The difference for Case 1-4 freezes at $t = 100$ m with a value >10%. The process for Case 1-5 is divided into two stages. First, as in Case 1-4, the difference Δ decreases until the water from the first rainfall period ends. Then, it remains constant between rainfall periods and decreases again during the second rainfall event.

In order to analyze in detail Case 1-5, a probe is set at $x = 1000$ m, as a representative point. The temporal evolution of infiltration rate and water depth for this point are plotted in Fig. 4(a) and (b) for Horton and Green–Ampt models, respectively. These plots show that, although both infiltration models present very similar behavior, the existence of temporal regions with $f = 0$ implies that the water is infiltrating for a period of time shorter than the one considered for the calibration process and, hence, the calibration is not correct.

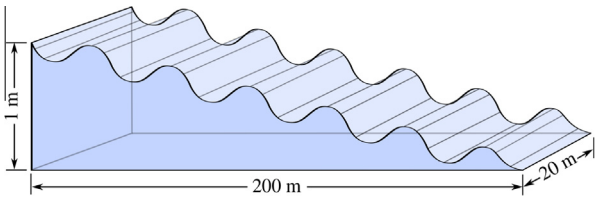

Fig. 8. Case 3 topography.

3.2.2. Slope and roughness variations

In this section, different slope and roughness combinations are studied in order to determine their influence in the difference between infiltration models. As in the previous section, the calibrated parameters under horizontal ponded soil conditions are used (Table 1). The effect of slope and roughness is studied by means of the mildness fraction of the plane, defined as the ratio between normal water depth h_N and critical water depth h_C. A rain discharge of (5 m^3/s) and 15,000 s of duration and three different values of h_N/h_C (2.33, 1.40 and 0.61) are set. In all these cases, the rain duration is such that surface water is available between $0 < t < 300$ min. Fig. 5 shows the overall numerical results. Fig. 5 (a) and (b) clearly shows that the outlet hydrographs and the final cumulative volumes for both infiltration models do not differ significantly when changing the mildness fraction. Therefore, in the

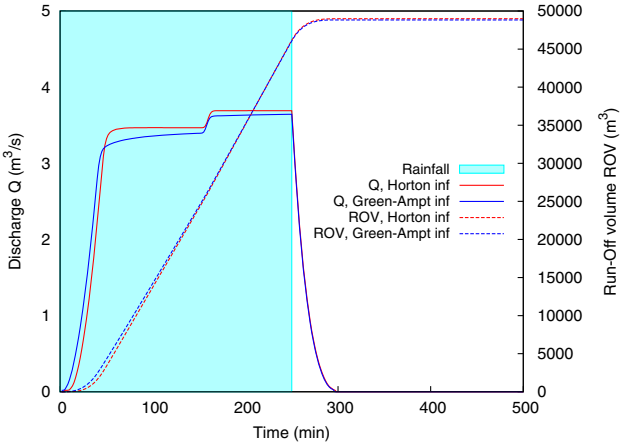

(a) Outlet discharge and runoff for Case 2-100.

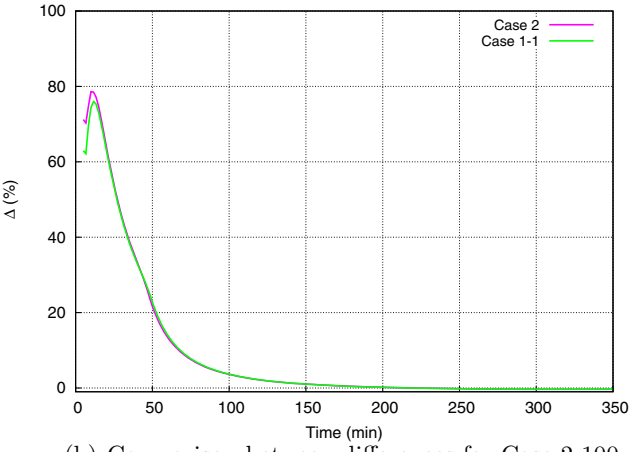

(b) Comparison between differences for Case 2-100.

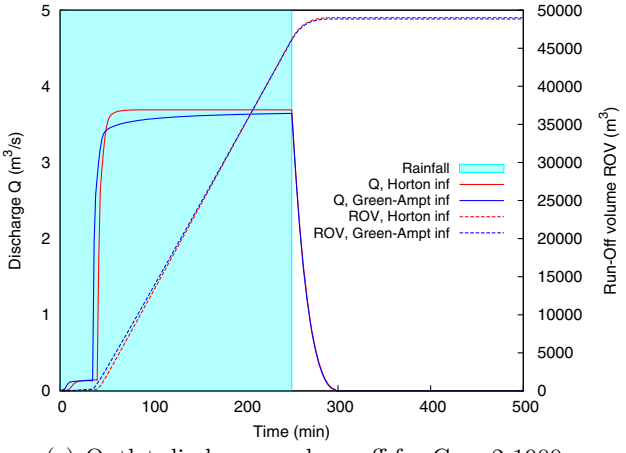

(c) Outlet discharge and runoff for Case 2-1900.

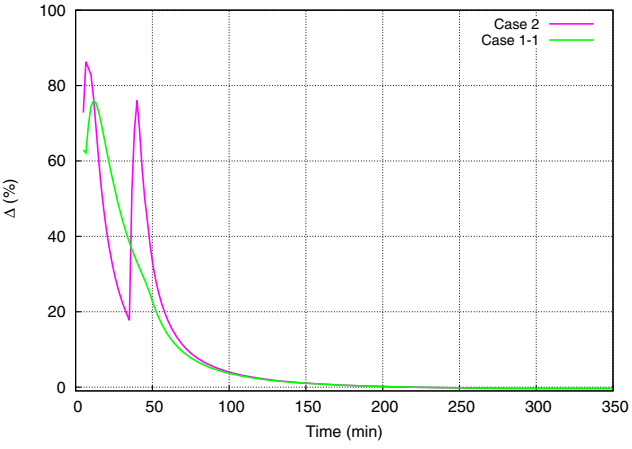

(d) Comparison between differences for Case 2-1900.

Fig. 7. Hydrographs and differences between infiltration models for Case 2.

light of the results, infiltration parameter calibration is not strongly dependent on the mildness fraction under full water supply.

3.3. Case 2: single storage area

Starting from the same topography used in the previous section, a trapezoidal furrow is added to the plane (see Fig. 6) acting as a storage depression. The purpose of this case is to check the changes in the outlet hydrographs and runoff volume curves due to the storage under different conditions and to extrapolate them to natural surfaces on real catchments which have depressions (local minima of the surface). The same initial and rainfall setup as in Case 1-1 are assumed in order to establish a comparison with that case of the infiltration calibration and how it is affected by a volume storage of $\approx$1000 m^3.

Table 3 summarizes the numerical cases presented in this section and Fig. 7 shows the numerical results and the comparison with the no-furrow situation, corresponding to Case 1-1.

In view of the results obtained, it is observed that the storage area does not generate significant difference between infiltration models in the outlet runoff volume. On the other hand, the time distribution of the outlet discharge is affected by the position of the furrow, being more significant the difference between infiltration models when the furrow is placed downstream (Case 2-1900, Fig. 7(d)). Hence, this test shows that the topography features can significantly affect the calibration of the infiltration parameters.

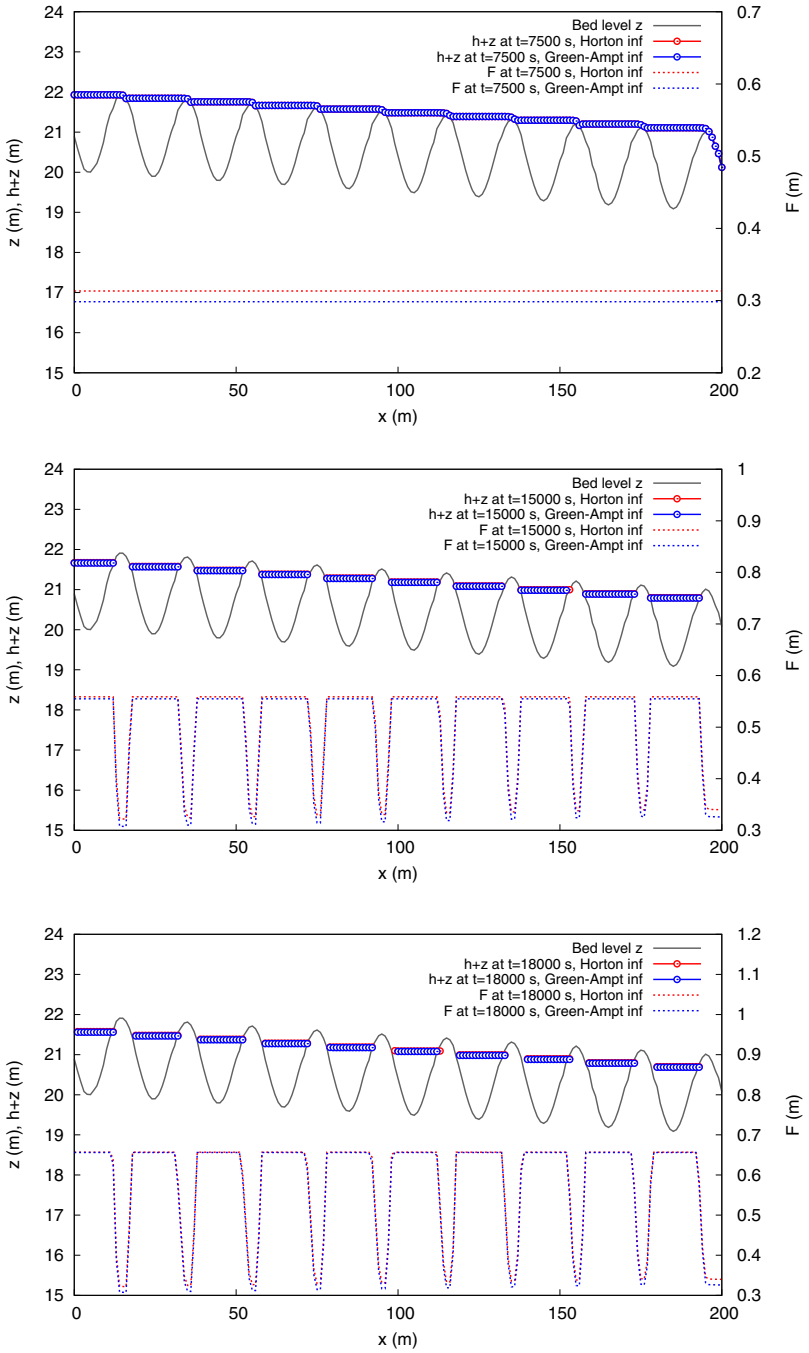

Fig. 9. Case 3. Longitudinal profiles at $t = 125$ min (upper), $t = 250$ min (middle) and $t = 300$ min (lower).

The evolution of the difference between infiltration models changes depending on the position of the furrow. In the case of the downstream furrow, a particular behavior is observed. Initially ($t < 40$ s) the outflow is generated only by rainfall downstream from the furrow, since runoff from upstream areas is stored in the furrow, filling it. The difference between infiltration models during this time behaves as in case 2-100, because, it is essentially identical. However, at $t \approx 40$ s the Green–Ampt hydrograph shows a sudden rise in outflow, indicating that the furrow has been filled. The Horton hydrograph rises somewhat later. This lag between the sudden increase in outflow generates the increase in difference between both infiltration models seen in Fig. 7(d), which goes almost to 80% (i.e., Green–Ampt produces a large outflow because the furrow has been filled, but Horton is still filling up the furrow). As soon as the Horton hydrograph initiates the rising outflow, both infiltration models are allowing runoff from the entire catchment to flow out, and therefore, as time advances, they tend to be identical.

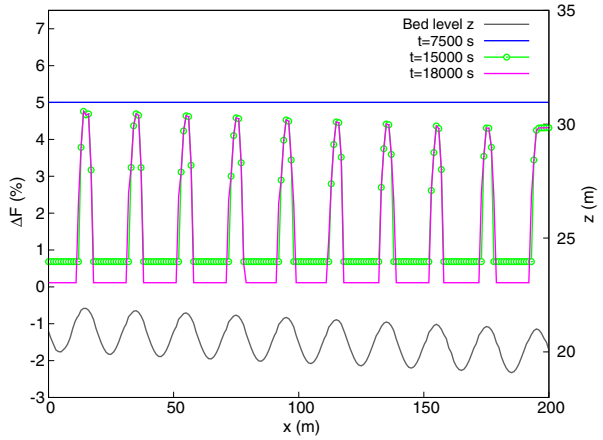

Fig. 10. Case 3. Relative difference in cumulative infiltration.

3.4. Case 3: several storage areas

Following from the previous cases and working towards real topography, a case with a very irregular topography is presented and the effect of these terrain irregularities over the infiltration calibration is analyzed. The domain dimensions are presented in Fig. 8 and the bed level is given by:

$$z = 21.0 + 1.0 \sin\left(\frac{\pi}{10}x\right) - 0.005x \tag{16}$$

This kind of domain provides a large storage capacity for incoming rainfall water in which a study of the influence of an irregular topography on the infiltration models can be carried out. For this particular case, a constant rain pulse of 0.25 mm/s is assumed over all the domain during 125 min. This particular rain duration guarantees that the local maxima of the domain will not be ponded

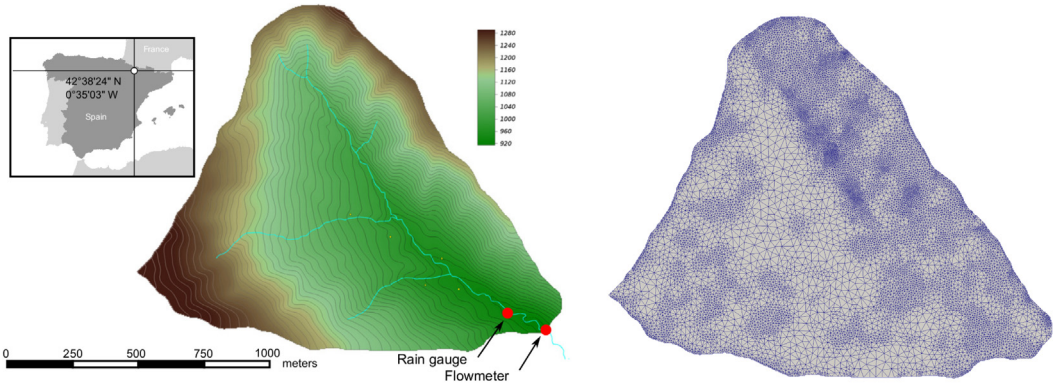

(a) Catchment location and hypsometry map.

(b) Catchment refined mesh.

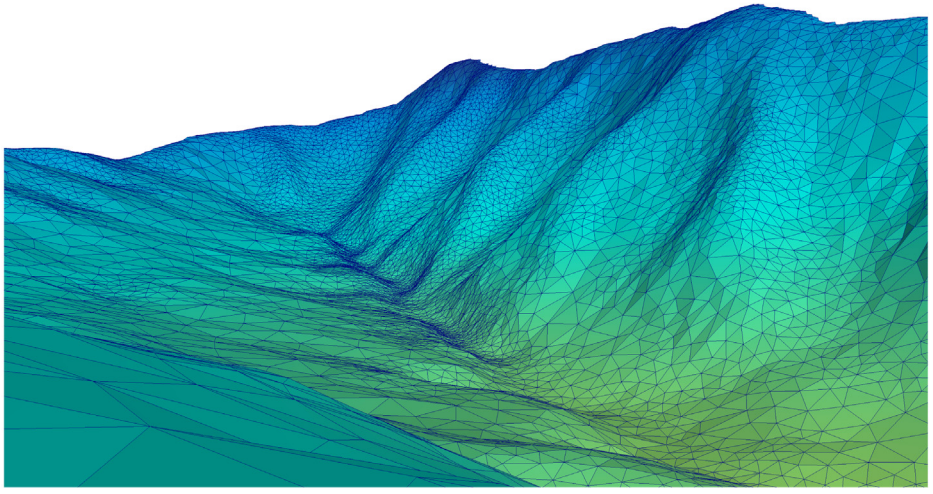

(c) Detail of the topography and the refined mesh (surface elevation is exaggerated 1.5x).

Fig. 11. Arnás catchment and mesh characteristics.

continuously so the fitting point ($t = 300$ min) is not reached (i.e., $F_H \neq F_{GA}$). On the other hand, the local minima are continuously ponded. This allows to observe differences between both regions. The same initial conditions and infiltration parameters (Table 1) as in previous cases are considered.

Fig. 9 shows the longitudinal profiles of the water level $h + z$ and cumulative infiltration F at $t = 125$ min, when rainfall stops, $t = 250$ min and $t = 300$ min. The relative differences in F between infiltration models are presented in Fig. 10 in terms of the magnitude $\Delta F(\%)$, defined as in Eq. (14).

As shown in Fig. 9 (upper), surface water is available for infiltration until $t = 125$ min, so the relative difference $\Delta F(\%)$ remains constant all along the domain. As stated in the previous cases, this difference is due to the large time lapse for reaching the time for which the parameters have been fitted in Case 0 (300 min). After this time, rainfall stops and the surface water runs downstream except for the water stored in the local minima producing ponded and non-ponded regions (Fig. 9 (middle)). In this situation, differences appear in the cumulative infiltration profile, since water continues infiltrating in the ponded areas but, obviously, no infiltration occurs in non-ponded regions. As shown in Fig. 10, $\Delta F(\%)$ is minimized for $t = 300$ min, leading to a relative difference less than 0.1% in the ponded regions. On the other hand, the water available for infiltration in local maxima has not been enough to reach the fitting point. It is worth to mention that these differences cannot be observed using lumped models, as they do not have a spatial resolution for considering transient ponded conditions. These kind of phenomena show the capabilities and the need for distributed models. These results also bring to light the influence of the topography in the calibration of empirical infiltration models, again highlighting the need for distributed models.

A similar 1D setup was simulated by Thompson et al. (2010) to study the effects of microtopography in runoff generation and infiltration. Microtopography in Thompson et al. (2010) is a sinusoidal variation of terrain surface over a background terrain slope, as in the case presented here. Thompson et al. (2010) found that microtopography (i.e., sinusoidal variations) largely increased infiltration when compared against the slope without microtopography, and such increase was reported as proportional to the amplitude of the microtopography. The results reported in Fig. 9 are consistent with the observations by Thompson et al. (2010) and also show the cause of such behavior. There is a clear separation of flow by the maximum elevations which favors long-residence-time ponding (the so-called regime A in Thompson et al. (2010)). Moreover, in the results shown here it can be seen that there is differential infiltration because of the "microtopographic variations" which may also be relevant in particular for parameter calibration, specially for mid-intensity rainfall in which ponding times are most relevant.

4. Application to a real catchment

The full shallow water model with infiltration is now applied to a real catchment in order to evaluate its quality by comparing the numerical results with the experimental data in two measured events. The wide range of test cases studied in previous sections provide some insight into the factors that may affect infiltration parameter calibration. Therefore, such insights are helpful to read into the hydrograph behavior and to identify properties of the catchment which may not be explicit in any way. In turn, such

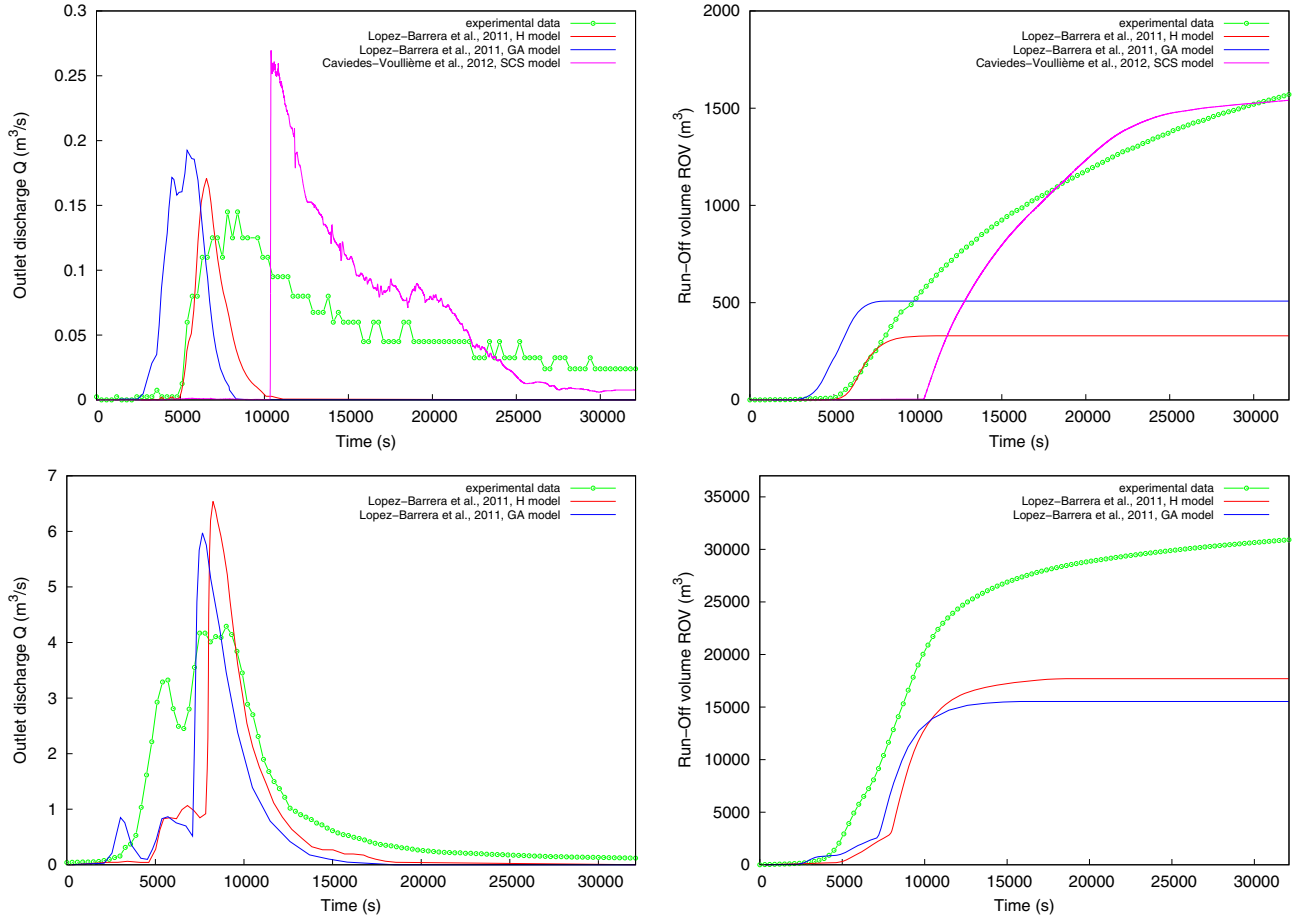

Fig. 12. Previous published results of the Arnás catchment simulation for two different events.

insights may aid in facilitating calibration of the infiltration parameters.

4.1. Catchment description and meshing

The Arnás catchment (2.84 km^2, 900–1340 m.a.s.l.) is located in the Northern Spanish Pyrenees, in the Borau valley (see Fig. 11(a)). From the geological point of view, the catchment lies over Eocene flysch bedrock and its land use has been changed along recent decades causing significant modifications in the vegetation cover, which ranges from patches of forest, dense bush areas, grassland meadows to bare land (García-Ruíz et al., 2005). Previous studies (García-Ruíz et al., 2005; Lana-Renault, 2007; Lana-Renault et al., 2007; Serrano-Pacheco, 2009) have provided information about soil types and vegetation mapping. This data conform the basis for the watershed characterization from a hydrological perspective.

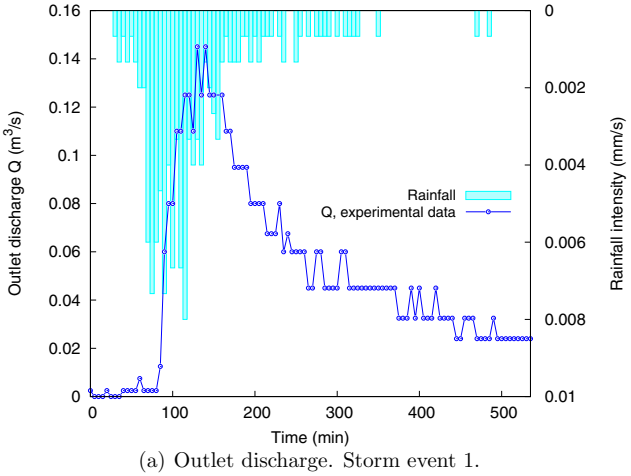

(a) Outlet discharge. Storm event 1.

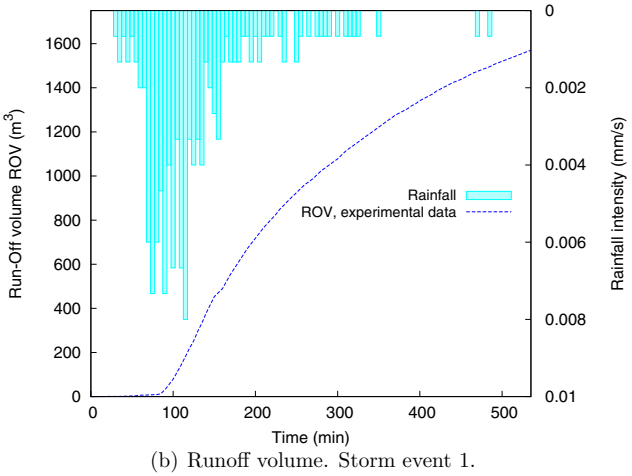

(b) Runoff volume. Storm event 1.

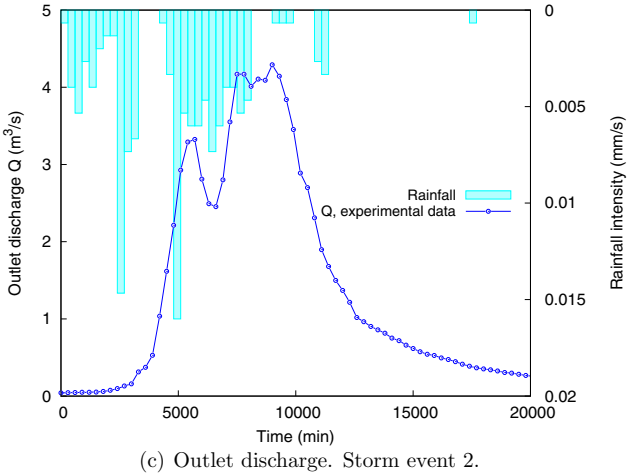

(c) Outlet discharge. Storm event 2.

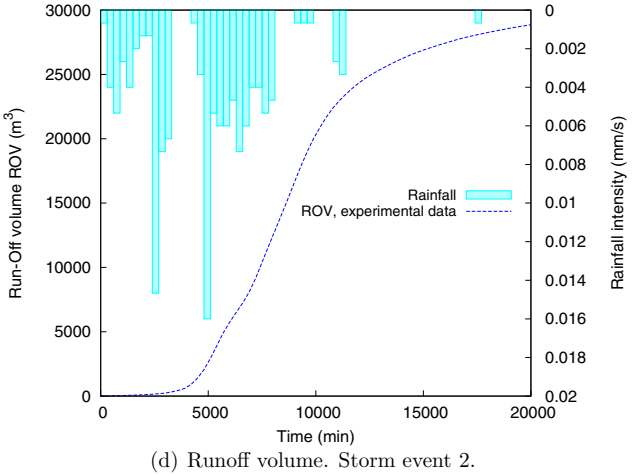

(d) Runoff volume. Storm event 2.

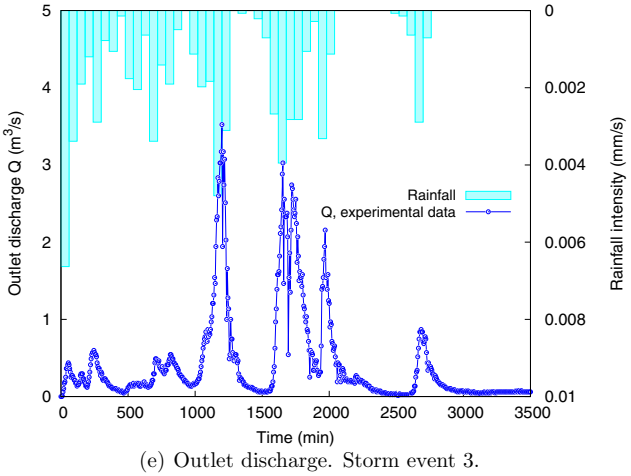

(e) Outlet discharge. Storm event 3.

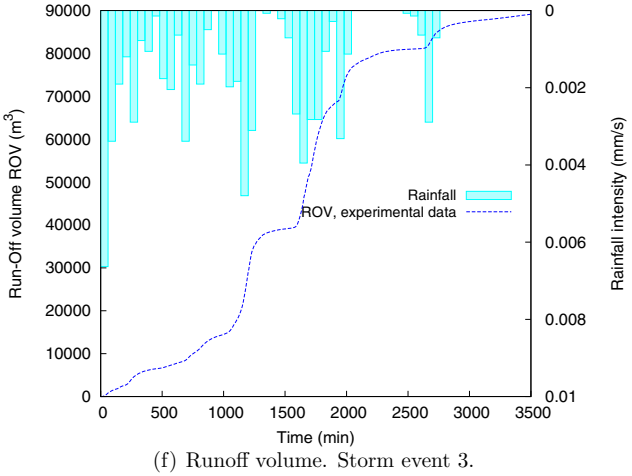

(f) Runoff volume. Storm event 3.

Fig. 13. Experimental hyetographs and hydrographs for Arnás basin.

Numerical simulation of this catchment was reported in López-Barrera et al. (2011) by means of a 2D diffusion wave distributed model for the surface flow and both Horton and Green–Ampt models for infiltration. This catchment was also simulated in Caviedes-Voullième et al. (2012) by means of the 2D shallow water equations together with the SCS-CN model for computing the precipitation loss. In both cases, some difficulties were found in reproducing the measured outlet hydrographs (see Fig. 12), which emphasizes the necessity of the careful study of the calibration and sensitivity analysis presented in previous sections. All the cited studies conclude that infiltration plays an important role in the catchment response due to the large precipitation losses.

Different types of meshing techniques for this catchment have been widely studied in Caviedes-Voullième et al. (2012), in order to find an optimal mesh for solving the SWE. The mesh used for simulating all the cases presented in this paper is shown in Fig. 11(b). A 3D representation of the catchment and the mesh is shown in Fig. 11(c).

4.2. Events description

In this paper, three events (referred to as Event 1, 2 and 3) are studied and compared with the experimental data. In all the cases, flow measurements were acquired at the outlet on the Arnás ravine (see Fig. 11(a)) with 5 min frequency. Rainfall was registered by a rain gauge with a frequency of 5 min for the events 1 and 2 and 60 min for the Event 3. Fig. 13 shows rainfall hyetographs, the measured outlet hydrograph and accumulated runoff volume for all the storm events.

4.3. Initial catchment water storage

As shown in previous sections of this paper (Cases 2 and 3), an important issue to take into consideration is the influence of the catchment surface water previous to the storm event. Logically, the relevance of the natural depressions depends on the rainfall volume, being specially important in the cases in which the outflow volume is comparable to the storage capacity of the catchment depressions. In order to appreciate the relevance of this water storage, two different simulations have been performed. The first one assumes zero surface water in the entire domain as initial condition. The second simulation starts considering that a previous storm has filled the local depressions of the catchment. Fig. 14 shows the results for an impervious situation, under three different rainfalls: synthetic uniform rain and the storm events 1 and 3. The results show that the depression has a similar effect on the hydrograph as in the synthetic cases previously shown in Fig. 7. This effect results negligible in the extreme rainfall event, due to the huge amount of rain volume compared to the depressions storage capacity.

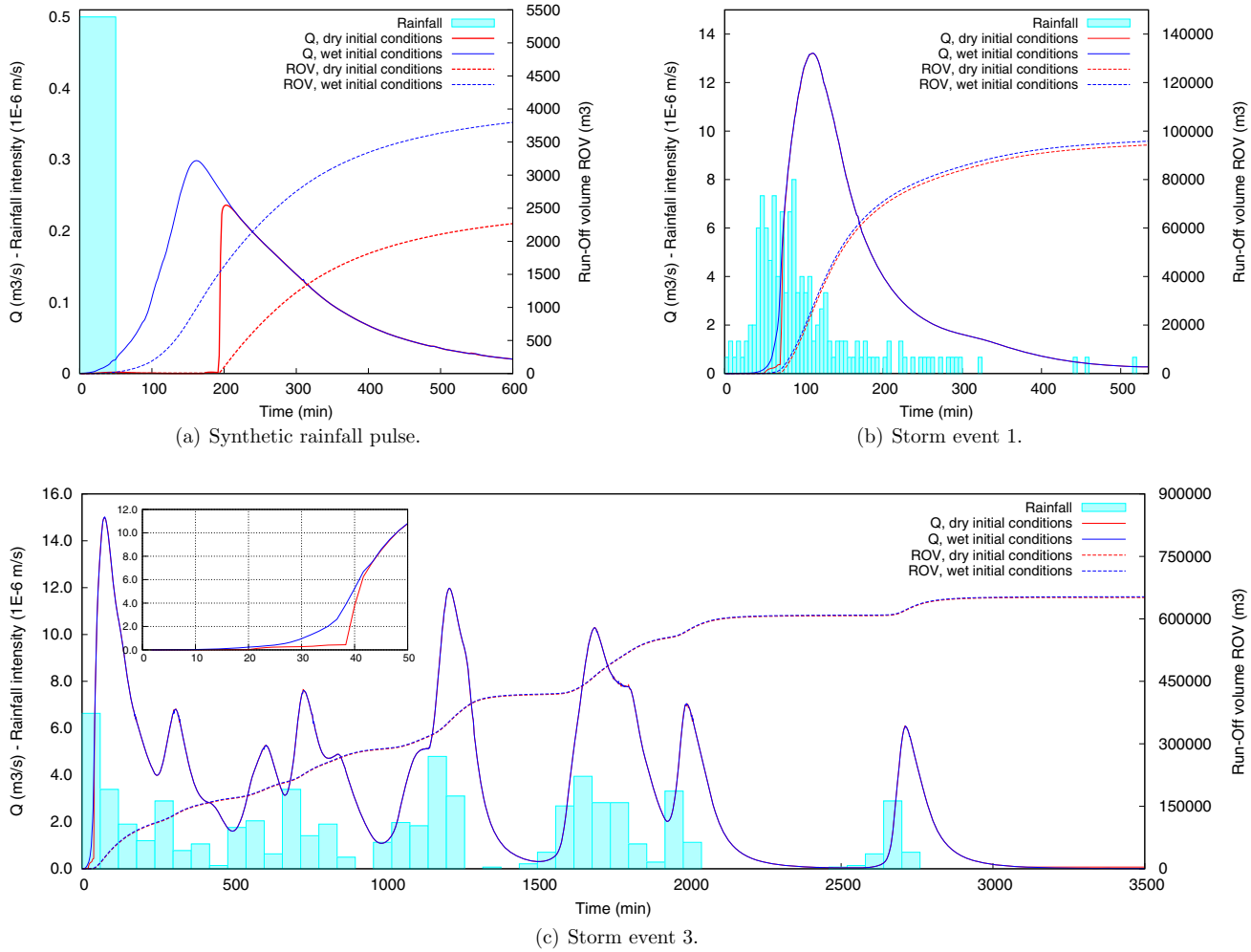

(a) Synthetic rainfall pulse.

(b) Storm event 1.

(c) Storm event 3.

Fig. 14. Effects of the initial water storage of the Arnás impervious catchment on the outlet hydrographs.

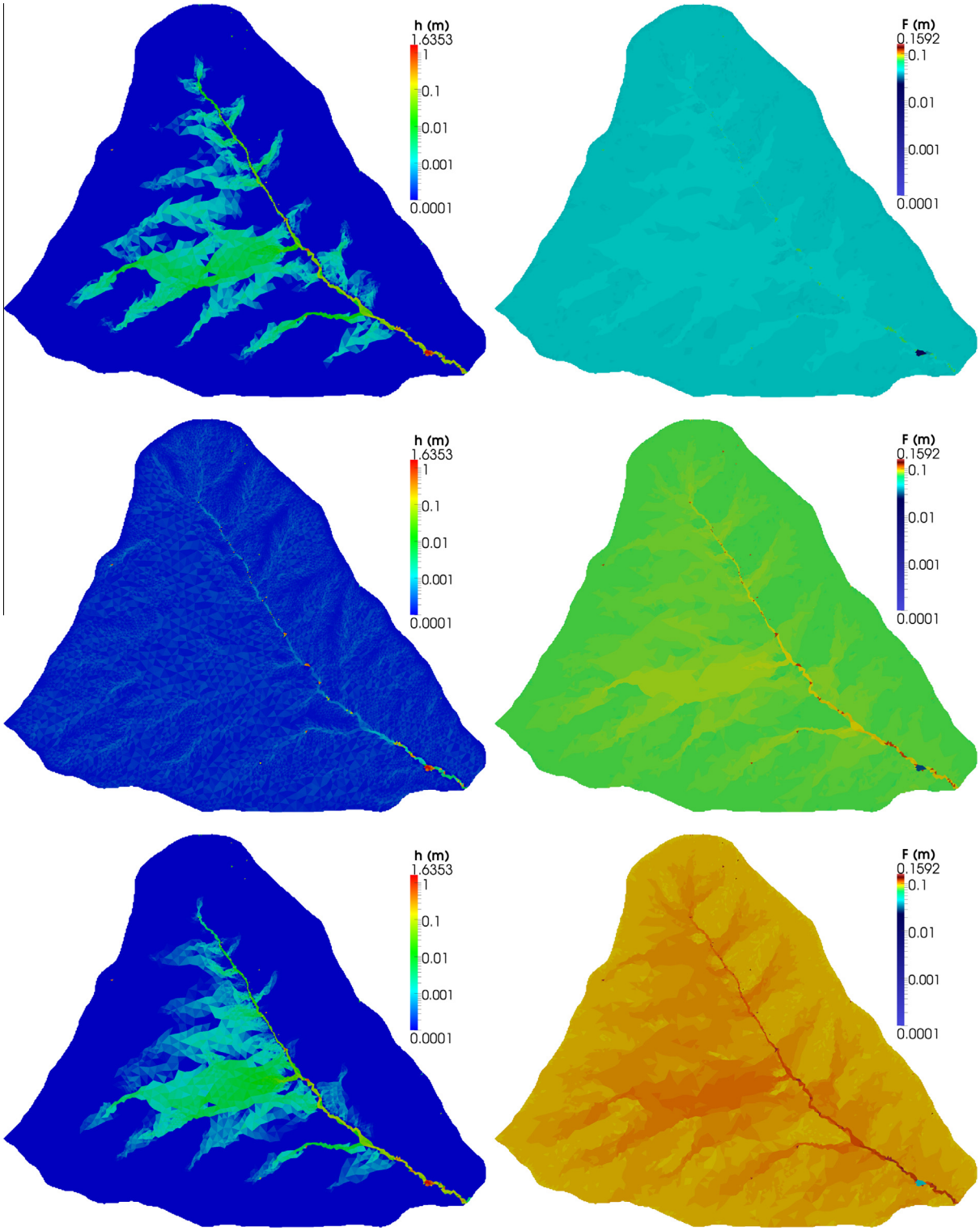

Fig. 15. Spatial distribution at catchment level of water depth (left) and cumulative infiltration (right) for the Event 3 at t = 12,000 s, t = 36,000 s and t = 50,000 s.

Table 4
Infiltration parameter set.

Event	Inf. model	Parameter 1	Parameter 2	Parameter 3
1	Horton	$k = 0.00026\ s^{-1}$	$f_c = 1.0 \cdot 10^{-7}$ m/s	$f_0 = 1.65 \cdot 10^{-5}$ m/s
1	Green–Ampt	$K = 0.8 \cdot 10^{-6}$ m/s	$\Psi = 0.0203$ m	$\Delta\theta = 3.5$
2	Horton	$k = 0.0001\ s^{-1}$	$f_c = 2.6 \cdot 10^{-6}$ m/s	$f_0 = 3.3 \cdot 10^{-6}$ m/s
2	Green–Ampt	$K = 8.0 \cdot 10^{-7}$ m/s	$\Psi = 0.01$ m	$\Delta\theta = 3.5$
3	Horton	$k = 0.0007\ s^{-1}$	$f_c = 2.0 \cdot 10^{-6}$ m/s	$f_0 = 3.5 \cdot 10^{-5}$ m/s
3	Green–Ampt	$K = 1.4 \cdot 10^{-6}$ m/s	$\Psi = 0.025$ m	$\Delta\theta = 2.0$

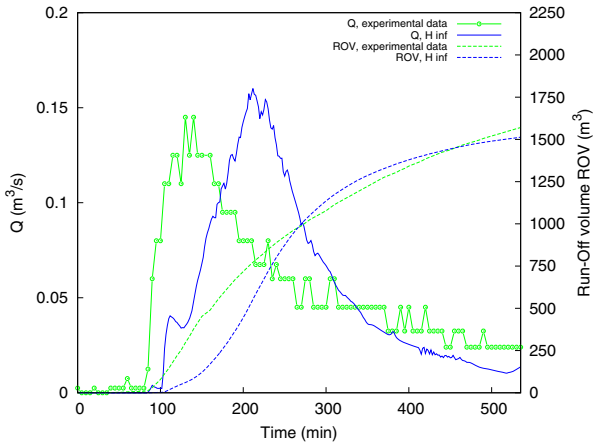

Fig. 16. Numerical vs. experimental data. Horton infiltration model. Storm event 1. IC = initial conditions.

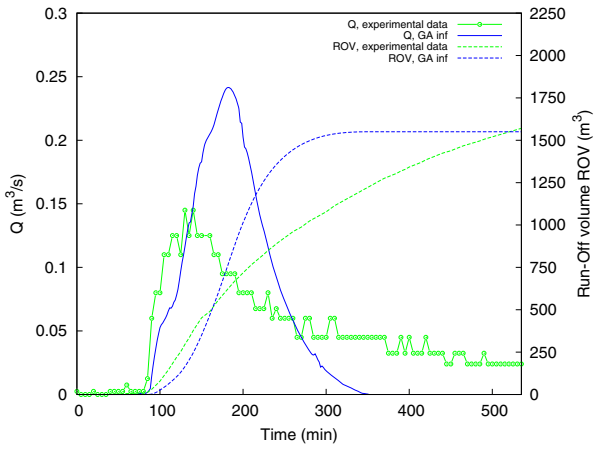

Fig. 17. Numerical vs. experimental data. Green–Ampt infiltration model. Storm event 1. IC = initial conditions.

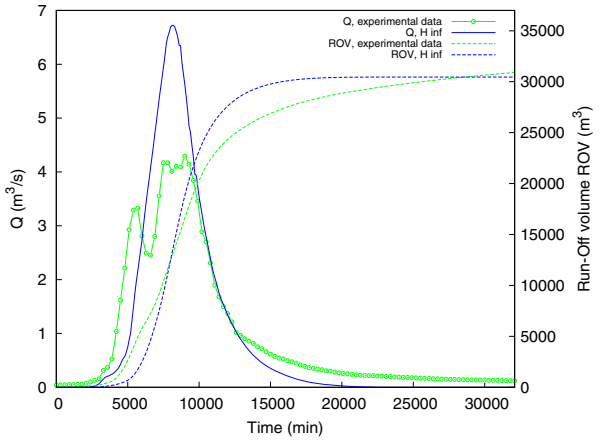

Fig. 18. Numerical vs. experimental data. Horton infiltration model. Storm event 2. IC = initial conditions.

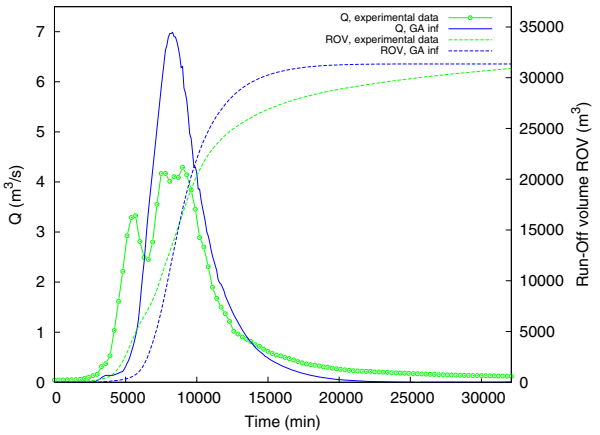

Fig. 19. Numerical vs. experimental data. Green–Ampt infiltration model. Storm event 2. IC = initial conditions.

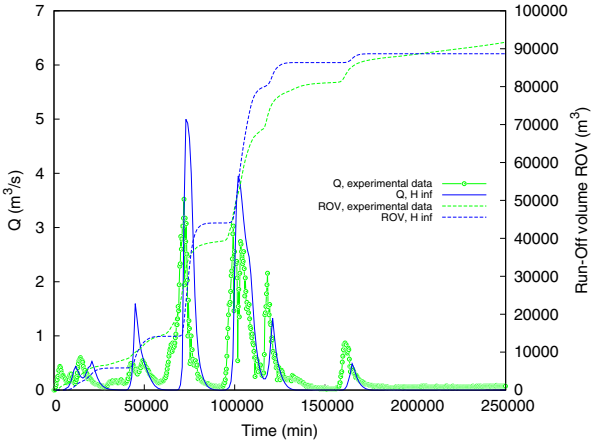

Fig. 20. Numerical vs. experimental data. Horton infiltration model. Storm event 3. IC = initial conditions.

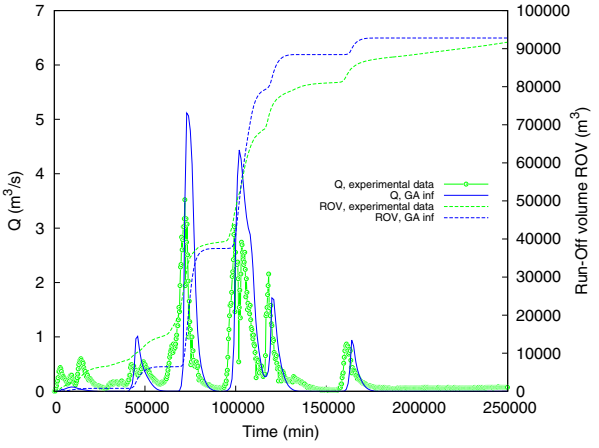

Fig. 21. Numerical vs. experimental data. Green–Ampt infiltration model. Storm event 3. IC = initial conditions.

4.4. Hydrograph fitting

By taking into account the previous considerations, an adjustment to the experimental data has been performed in the events presented in Fig. 13. In terms of surface water, the catchment initial state is an unknown but it can be inferred by comparing the rising limb shape of the experimental hydrographs with the ones obtained in the previous section (Fig. 14). In the light of this comparison, it has been assumed that the local depressions of the catchment have been filled by previous rains.

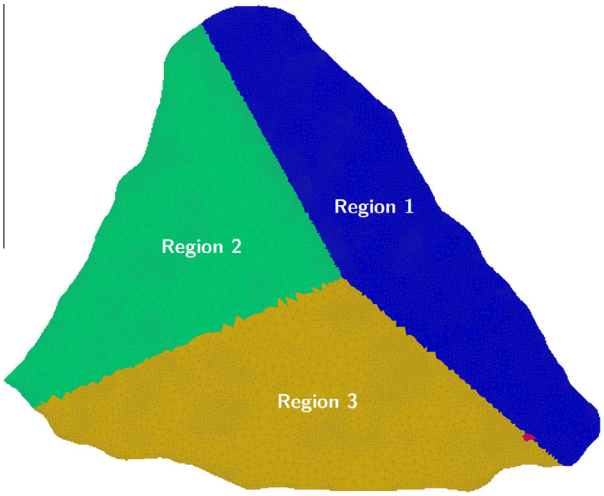

Fig. 22. Infiltration map based on the soil types.

As an illustrative example, Fig. 15 shows the spatial distribution of the water depth and cumulative infiltration on the whole catchment at three different times for the Event 3. This points out the relevance of using a distributed model for surface flow and infiltration computation, since there are significant differences ($\sim 300\%$ in cumulative infiltration) among catchment regions. Figs. 16–21 show the numerical results. Table 4 summarizes the infiltration parameters for all the events and both models. An overall good agreement between numerical and experimental results is observed for both Horton and Green–Ampt models. Both reproduce correctly the outflow volume which has been taken as the most relevant property of the catchment's response. In the case of Horton model results, the shape and peak value of the experimental hydrograph are also achieved with a certain delay in time. This is not so noticeable in the Green–Ampt results, but the peak value is not correctly reproduced in this case. Hence, despite the mostly good numerical results, some adjustments seem still to be necessary.

4.5. Infiltration mapping

In order to try to improve the agreement between numerical and experimental results and achieve a better experimental fitting, an infiltration map based on the catchment soil types has been designed (see Fig. 22). Three different regions are considered. The parameters used in the previous section are taken as starting point. This mapping allows to consider several regions infiltrating at different rates, which can be determining if the catchment has clearly different soil types, as in the considered case. Tables 5–7 show the best maps achieved and the infiltration parameters corresponding to each region. Figs. 23–28 show the numerical results. A considerable improvement in the shape of the outlet hydrographs is reached by the use of infiltration mapping, specially for the earlier time of the storm. Furthermore, the delay of the peak discharge in Horton model is partially corrected. Green–Ampt model also takes benefit from the infiltration mapping, specially in the storm event 3, in which the first discharge peaks are significantly better reproduced than when a single infiltration zone is used.

Table 5
Infiltration parameters re-fitting with infiltration map for Event 1.

Area	Inf. model	Parameter 1	Parameter 2	Parameter 3
Map H01 Region 1	H	$k = 0.00026\ \mathrm{s}^{-1}$	$f_c = 8.0 \cdot 10^{-9}\ \mathrm{m/s}$	$f_0 = 1.85 \cdot 10^{-5}\ \mathrm{m/s}$
Map H01 Region 2	H	$k = 0.00026\ \mathrm{s}^{-1}$	$f_c = 1.0 \cdot 10^{-7}\ \mathrm{m/s}$	$f_0 = 1.75 \cdot 10^{-5}\ \mathrm{m/s}$
Map H01 Region 3	H	$k = 0.00026\ \mathrm{s}^{-1}$	$f_c = 1.0 \cdot 10^{-7}\ \mathrm{m/s}$	$f_0 = 1.55 \cdot 10^{-5}\ \mathrm{m/s}$
Map GA01 Region 1	GA	$K = 7.65 \cdot 10^{-7}\ \mathrm{m/s}$	$\Psi = 0.02\ \mathrm{m}$	$\Delta\theta = 3.5$
Map GA01 Region 2	GA	$K = 2.3 \cdot 10^{-6}\ \mathrm{m/s}$	$\Psi = 0.05\ \mathrm{m}$	$\Delta\theta = 3.5$
Map GA01 Region 3	GA	$K = 8.0 \cdot 10^{-7}\ \mathrm{m/s}$	$\Psi = 0.02\ \mathrm{m}$	$\Delta\theta = 3.5$

Table 6
Infiltration parameters re-fitting with infiltration map for Event 2.

Area	Inf. model	Parameter 1	Parameter 2	Parameter 3
Map H01 Region 1	H	$k = 0.0001\ \mathrm{s}^{-1}$	$f_c = 1.0 \cdot 10^{-6}\ \mathrm{m/s}$	$f_0 = 3.3 \cdot 10^{-6}\ \mathrm{m/s}$
Map H01 Region 2	H	$k = 0.0001\ \mathrm{s}^{-1}$	$f_c = 4.7 \cdot 10^{-4}\ \mathrm{m/s}$	$f_0 = 5.9 \cdot 10^{-4}\ \mathrm{m/s}$
Map H01 Region 3	H	$k = 0.0001\ \mathrm{s}^{-1}$	$f_c = 1.0 \cdot 10^{-6}\ \mathrm{m/s}$	$f_0 = 1.9 \cdot 10^{-6}\ \mathrm{m/s}$
Map GA01 Region 1	GA	$K = 3.0 \cdot 10^{-7}\ \mathrm{m/s}$	$\Psi = 0.01\ \mathrm{m/s}$	$\Delta\theta = 3.5$
Map GA01 Region 2	GA	$K = 1.0 \cdot 10^{-6}\ \mathrm{m/s}$	$\Psi = 0.06\ \mathrm{m/s}$	$\Delta\theta = 3.5$
Map GA01 Region 3	GA	$K = 7.0 \cdot 10^{-7}\ \mathrm{m/s}$	$\Psi = 0.01\ \mathrm{m/s}$	$\Delta\theta = 3.5$

Table 7
Infiltration parameters re-fitting with infiltration map for Event 3.

Area	Inf. model	Parameter 1	Parameter 2	Parameter 3
Map H01 Region 1	H	$k = 0.0007\ \mathrm{s}^{-1}$	$f_c = 2.0 \cdot 10^{-6}\ \mathrm{m/s}$	$f_0 = 3.5 \cdot 10^{-5}\ \mathrm{m/s}$
Map H01 Region 2	H	$k = 0.0007\ \mathrm{s}^{-1}$	$f_c = 2.0 \cdot 10^{-6}\ \mathrm{m/s}$	$f_0 = 3.5 \cdot 10^{-5}\ \mathrm{m/s}$
Map H01 Region 3	H	$k = 0.0007\ \mathrm{s}^{-1}$	$f_c = 2.0 \cdot 10^{-6}\ \mathrm{m/s}$	$f_0 = 2.5 \cdot 10^{-5}\ \mathrm{m/s}$
Map GA01 Region 1	GA	$K = 1.8 \cdot 10^{-6}\ \mathrm{m/s}$	$\Psi = 0.025\ \mathrm{m/s}$	$\Delta\theta = 2.0$
Map GA01 Region 2	GA	$K = 1.8 \cdot 10^{-6}\ \mathrm{m/s}$	$\Psi = 0.025\ \mathrm{m/s}$	$\Delta\theta = 2.0$
Map GA01 Region 3	GA	$K = 1.0 \cdot 10^{-6}\ \mathrm{m/s}$	$\Psi = 0.025\ \mathrm{m/s}$	$\Delta\theta = 2.0$

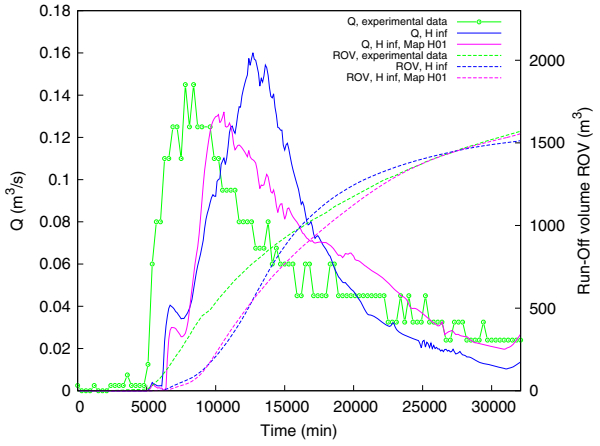

Fig. 23. Event 1 parameter re-fitting with infiltration map. Horton infiltration model.

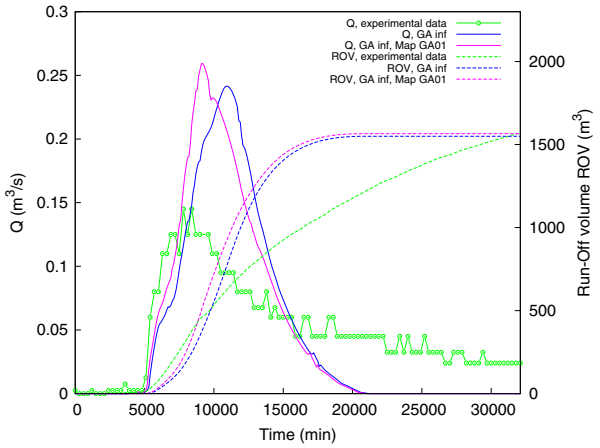

Fig. 24. Event 1 parameter re-fitting with infiltration map. Green–Ampt infiltration model.

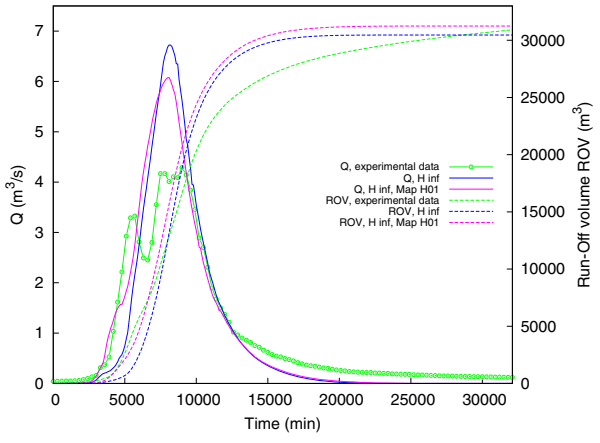

Fig. 25. Event 2 parameter re-fitting with infiltration map. Horton infiltration model.

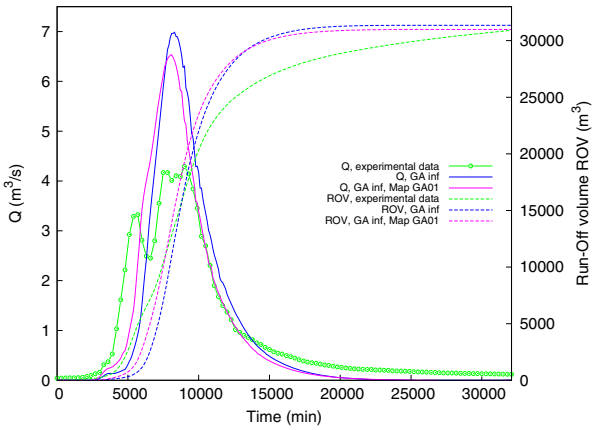

Fig. 26. Event 2 parameter re-fitting with infiltration map. Green–Ampt infiltration model.

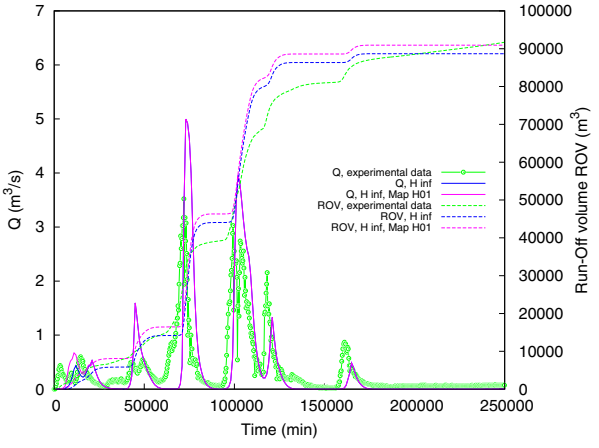

Fig. 27. Event 3 parameter re-fitting with infiltration map. Horton infiltration model.

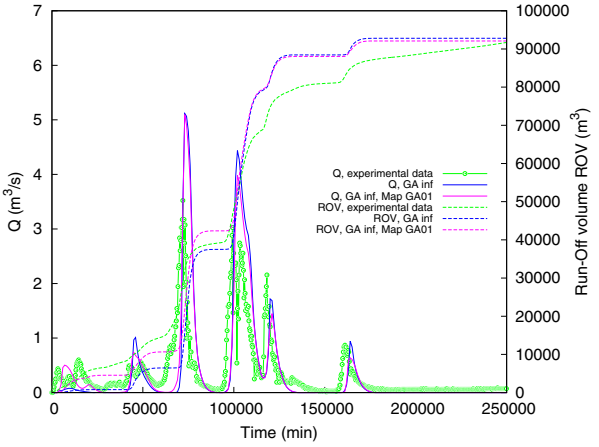

Fig. 28. Event 3 parameter re-fitting with infiltration map. Green–Ampt infiltration model.

4.6. Overall results

In this section, a brief summary of the numerical results is presented together with the comparison with the previous published results for events 1 and 2 (Figs. 29 and 30). The results corresponding to Event 1 show a significant improvement compared to the results from López-Barrera et al. (2011) and Caviedes-Voullième et al. (2012). In the first case, the authors aim was to fit the hydrograph peak discharge giving a minor importance to the outlet runoff volume (Fig. 29, right). On the other hand, Caviedes-Voullième et al. (2012) follows a completely different strategy, considering

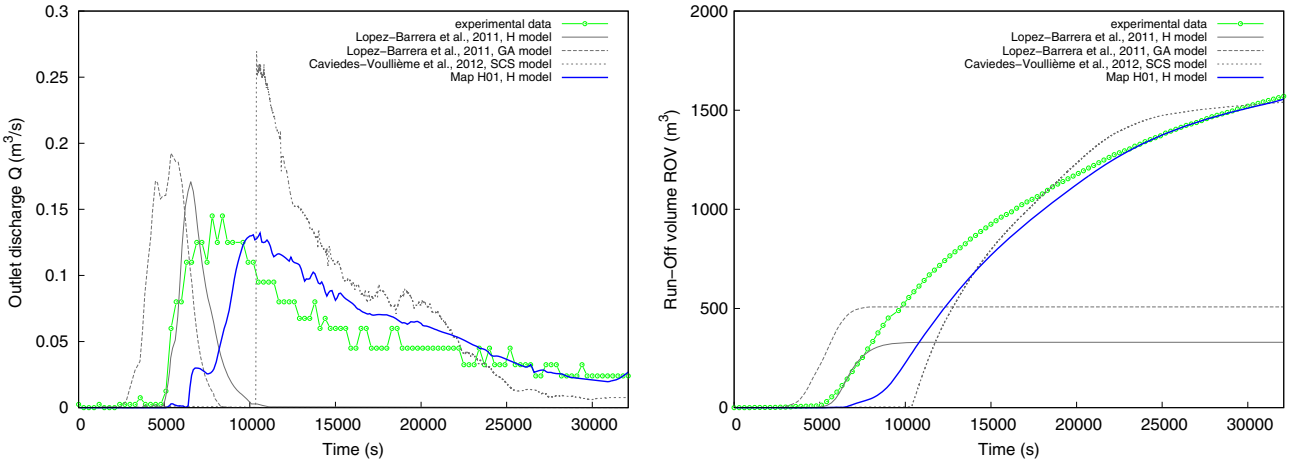

Fig. 29. Comparison between the previous publications and the best fitting obtained in this work for the Event 1.

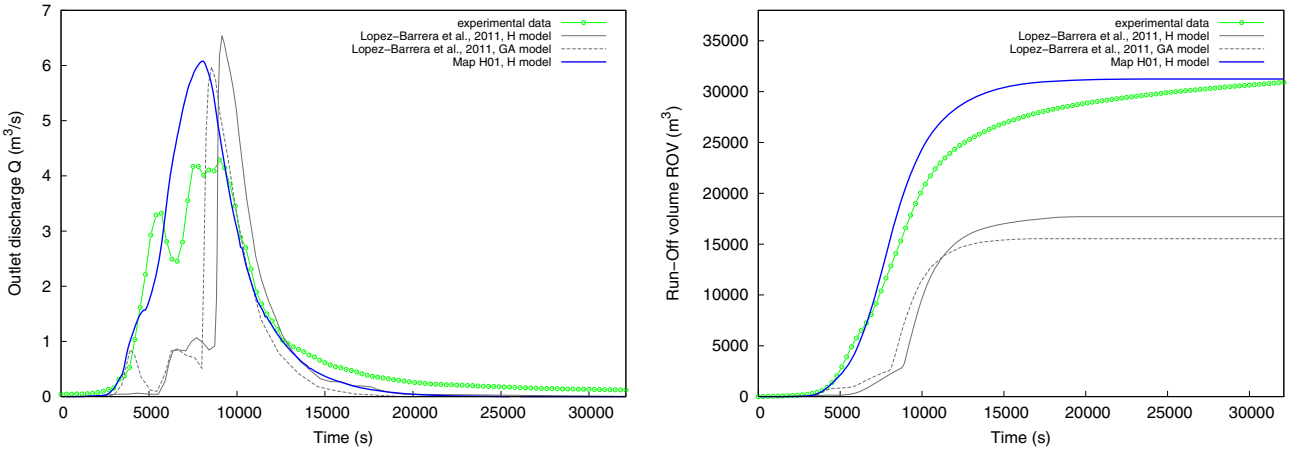

Fig. 30. Comparison between the previous publications and the best fitting obtained in this work for the Event 2.

that the runoff volume is the most important variable to fit (Fig. 29, right). The numerical results presented in the present work provide an overall good fit to the experimental outlet hydrograph and match perfectly the runoff volume.

The adjustment presented in López-Barrera et al. (2011) for Event 2 follows the same criterion of fitting the peak discharge, providing an incorrect fit of the outlet runoff volume (Fig. 30, right). The results obtained in this work fit accurately the rising and recession limbs of the experimental hydrograph (Fig. 30, left) and match the runoff volume (Fig. 30, right).

As a further improvement, the interflow component might improve the fitting of our numerical and experimental peak discharges. However it is not clear that interflow, and the associated exfiltration, was relevant in Arnas according to the field observations. However, in case of including that component, the strategy suggested in Simons et al. (2014) could be a starting point but it involves calibration of an extra parameter apart from the infiltration parameters. Furthermore, they should be simultaneously and not sequentially calibrated to be correct.

5. Conclusions

The implementation of a full shallow water model with empirical infiltration techniques has been presented in this work. The volume losses due to infiltration have been computed in a spatially and temporally distributed way by means of the empirical laws of Horton and Green–Ampt, which require parameters to be properly calibrated. In the first part of this work, both infiltration models are calibrated in a horizontal ponded soil in order to produce the same cumulative infiltration at the end of a given time. Afterwards, the influence of the storm and topography on the runoff and, hence, on this calibration has been studied. In the light of the results, several conclusions have been reached:

- The calibration performed under flat soil conditions to achieve the same cumulative infiltration in both models at a given time is not significantly affected by the introduction of a slope if the calibration point is respected. In other words, the period of time with available water in the slope should be approximately the same for what the calibration has been performed in order to preserve its validity. In general terms, the greater the difference between water availability time and calibration time, the greater the difference between infiltration models.
- Bed slope and roughness variations do not affect significantly the calibration process provided that there is enough available surface water.
- It has been shown that the differences in runoff volume between infiltration models is not affected by the presence of a furrow with a considerable storage capacity. On the other hand, the temporal distribution of the water discharge seems to be sensitive to this, especially when the furrow is located downstream.

- When the topography presents a set of storage depressions, differences appear in the cumulative infiltration profiles, since water continues infiltrating in the ponded areas, even when rainfall stops. These differences cannot be reproduced by a lumped model. Hence, this case points out the need for distributed models when simulating this kind of topographies.

All these individual results lead to an overall conclusion: the topography and rainfall features have influence in the calibration of the infiltration parameters for Horton and Green–Ampt models. Hence, a single set of parameters cannot accurately model the infiltration process on a given soil.

The simulation of a real catchment has been carried out for two storm events in the second part of this article. A good agreement between numerical and experimental data has been observed for both Horton and Green–Ampt models, specially for the extreme rainfall event, due to its higher water volume. From this part of the work, the conclusion are as follows:

- Infiltration parameters of the catchment (for both models) depend on the storm pattern and the initial ponded water in the basin. Hence they should be calibrated depending on the rainfall characteristics and initial conditions.
- An infiltration map which considers different soil types improves significantly the agreement between numerical and experimental hydrographs in both infiltration models.

In general terms, the calibration of the empirical infiltration models studied in this paper, Horton and Green–Ampt methods, present a significant improvements over previous published results corresponding to the Arnás basin. The reason for this good agreement between numerical and experimental data is the careful study concerning the initial state of the catchment, in terms of surface water, and the infiltration mapping in several areas performed in Section 4.5.

The full 2D shallow water model for the surface flow calculation allows to improve the numerical results in two ways. On the one hand, the coupling of Horton and Green–Ampt models with a 2D surface flow model confers the possibility of calculating the soil infiltration rate locally for each cell. On the other hand, it is shown that the possibility of using infiltration maps in order to take into account different soil or vegetation types improves the quality of the results.

Acknowledgement

The present work was partially funded by the Aragón Government through the Fondo Social Europeo.

References

ASCE, 1996. Hydrology Handbook, second ed. American Society of Civil Engineers (ASCE).
Caviedes-Voullième, D., García-Navarro, P., Murillo, J., 2012. Influence of mesh structure on 2D full shallow water equations and SCS Curve Number simulation of rainfall/runoff events. J. Hydrol. 448–449, 39–59.
Cea, L., Garrido, M., Puertas, J., 2010. Experimental validation of two-dimensional depth-averaged models for forecasting rainfall–runoff from precipitation data in urban areas. J. Hydrol. 382, 88–102.
Chu, S., 1978. Infiltration during an unsteady rain. Water Resour. Res. 14, 461–466.
Esteves, M., Faucher, X., Galle, S., Vauclin, M., 2000. Overland flow and infiltration modelling for small plots during unsteady rain: numerical results versus observed values. J. Hydrol. 228, 265–282.
García-Ruíz, J., Arnáez, J., Beguería, S., Seeger, M., Martí-Bono, C., Regüés, D., Lana-Renault, N., White, S., 2005. Runoff generation in an intensively disturbed, abandoned farmland catchment, central spanish pyrenees. Catena 59, 79–92.
Green, W., Ampt, G., 1911. Studies on soil physics: 1. Flow of air and water through soils. J. Agric. Sci. 4, 1–24.
Horton, R., 1933. The role of infiltration in the hydrologic cycle. Trans. Am. Geophys. Union 14, 446–460.
Horton, R., 1939. Analysis of runoff plot experiments with varying infiltration capacities. Trans. Am. Geophys. Union 20, 683–694.
Kale, R., Sahoo, B., 2011. Green–Ampt infiltration models for varied field conditions: a revisit. Water Resour. Manage. 25, 3505–3536.
Kim, D., Seo, Y., 2013. Hydrodynamic analysis of storm movement effects on runoff hydrographs and loop-rating curves of a v-shaped watershed. Water Resour. Res. 49, 6613–6623.
Lana-Renault, N., 2007. Respuesta hidrológica y sedimentológica en una cuenca de montaa media afectada por cambios de cubierta vegetal: la cuenca experimental de Arnás, Pirineo Central. Ph.D. Thesis. Universidad de Zaragoza.
Lana-Renault, N., Latron, J., Reguees, D., 2007. Streamflow response and water-table dynamics in a sub-mediterranean research catchment (central pyrenees). J. Hydrol. 347, 497–507.
López-Barrera, D., García-Navarro, P., Brufau, P., 2011. Sources of uncertainty in the validation of a coupled hydrological-hydraulic simulation model with sediment transport. La Houille Blanche 3, 17–22.
Mein, R.G., Larson, C.L., 1973. Modeling infiltration during a steady rain. Water Resour. Res. 9, 384–394.
Migliaccio, K., Srivastav, P., 2007. Hydrologic components of watershed-scale models. Trans. ASABE 50, 1695–1703.
Murillo, J., García-Navarro, P., 2010. Weak solutions for partial differential equations with source terms: application to the shallow water equations. J. Comput. Phys. 229, 4327–4368.
Murillo, J., García-Navarro, P., Burguete, J., Brufau, R., 2007. The influence of source terms on stability, accuracy and conservation in two-dimensional shallow flow simulation using triangular finite volumes. Int. J. Numer. Methods Fluids 54, 543–590.
Philip, J.R., 1969. Theory of infiltration. Adv. Hydrosci. 5, 215–296.
Rawls, W., Brakensiek, D., 1983. A procedure to predict Green and Ampt infiltration parameters. In: Proceeding of ASAE conferences on advances in infiltration, Chicago, Illinois, pp. 102–112.
Rawls, W., Yates, P., Asmussen, L., 1976. Calibration of Selected Infiltration Equation for the Georgia Coastal Plain. Report ARS-S-113. Agriculture Research Service.
Richards, L.A., 1931. Capillary conduction of liquids through porous mediums. J. Appl. Phys. 1 (5), 318–333.
Serrano-Pacheco, A., 2009. Simulación numérica bidimensional de procesos hidrológicos e hidráulicos sobre lecho irregular deformable. Ph.D. Thesis. Universidad de Zaragoza.
Simons, F., Busse, T., Hou, J., Özgen, I., Hinkelmann, R., 2014. A model for overland flow and associated processes within the Hydroinformatics Modelling System. J. Hydroinform. 16 (2), 375–391.
Singh, V., Woolhiser, D., 2002. Mathematical modeling of watershed hydrology. J. Hydrol. Eng. 7, 270–292.
Te Chow, V., Maidment, D., Mays, L., 1988. Applied Hydrology. McGraw-Hill Civil Engineering Series. MCGRAW-HILL Higher Education.
Thompson, S., Katul, G., Porporato, A., 2010. Role of microtopography in rainfall–runoff partitioning: an analysis using idealized geometry. Water Resour. Res. 46 (W07520).
United States Department of Agriculture (USDA), 1986. Urban Hydrology for Small Watersheds. Environment Agency Report.
Van den Putte, A., Govers, G., Leys, A., Langhans, C., Clymans, W., Diels, J., 2013. Estimating the parameters of the Green–Ampt infiltration equation from rainfall simulation data: why simpler is better. J. Hydrol. 476, 332–344.